JOURNAL OF THERMOPHYSICS AND HEAT TRANSFER
Vol. 15, No. 2, April–June 2001

Vibration–Dissociation Coupling Using Master Equations in Nonequilibrium Hypersonic Blunt-Body Flow

Eswar Josyula*
U.S. Air Force Research Laboratory, Wright–Patterson Air Force Base, Ohio 45433-7521
and
William F. Bailey†
U.S. Air Force Institute of Technology, Wright–Patterson Air Force Base, Ohio 45433-7521

Numerical simulations are presented of a steady-state hypersonic flow past a hemisphere cylinder. Two types of models, one a lumped Landau–Teller vibrational relaxation model (Landau, L., and Teller, E., "Zur Theorie der Schalldispersion," *Physikalalische Zeitschrift der Sowjetunion*, Vol. 10, No. 1, 1936, pp. 34–43) and the other a discrete state kinetic relaxation model (DSKR), were used to study effects of vibration–dissociation coupling on the flow physics. The widely used Park's dissociation model was used as baseline for coupling vibration and dissociation processes (Park, C., *Nonequilibrium Hypersonic Aerothermodynamics*, Wiley, New York, 1990, p. 114). For a Mach 8.6 flow, both relaxation models matched experimental data. At Mach 11.18, however, the underprediction of shock-standoff distance by both relaxation models using Park's model for dissociation coupling provided the motivation to implement a new master equation-based (DSKR) depletion model. The new model was used to study the effect of dissociation on population depletion in the vibrational states of the nitrogen molecule. The new model helps explain the restricted success of Park's dissociation model in certain temperature ranges of hypersonic flow past a blunt body. In the range of 5000–15,000 K, the new model yielded a substantial rate reduction relative to Park's equilibrium rate at lower temperatures and a consistent value at the high end. Application of the new model to a Mach 19.83 flow at reentry conditions resulted in an increase in the shock-standoff distance.

Nomenclature

D_e = potential well depth
e = total energy per unit mass
h = enthalpy, Planck's constant
i, j = species indices in quantum levels v, w
k = Boltzmann constant
M = Mach number, molecular weight
p = pressure
$\dot{\boldsymbol{q}}$ = heat flux vector
r = nose radius
St = Stanton number, $\boldsymbol{n} \cdot \dot{\boldsymbol{q}}/\rho_\infty u_\infty (h_\infty - h_{\text{wall}})$
s = species O_2, N_2, O, N, subscript
T = translational temperature
T_{fl} = first-level vibrational temperature
T_v = vibrational temperature for which population densities correspond to a Boltzmann
$\boldsymbol{u}$ = velocity vector
$\boldsymbol{u}_s$ = diffusion velocity vector for species s
$\boldsymbol{u}_{vs}$ = diffusion velocity vector for level v for species s
v, w = vibrational quantum numbers
x, y = Cartesian coordinates
γ = ratio of specific heats
ϵ = quantum level energy
Θ_d = characteristic temperature of dissociation
Θ_v = characteristic temperature of vibration
θ = angular spacing, deg
ρ = mixture density
ρ_s = density of species s
ρ_v = state density in the vth vibrational level
τ = relaxation time
$\tilde{\tau}$ = shear stress
φ_l = deviation of last vibrational level, dissociating state
φ_v = deviation of quasi-steady distribution from an equilibrium Boltzmann
∞ = freestream conditions, subscript

Presented as Paper 2000-2261 at the AIAA 31st Plasmadynamics and Lasers Conference, Denver, CO, 19–22 June 2000; revision received 7 December 2000; accepted for publication 7 December 2000.

*Research Aerospace Engineer, Air Vehicles Directorate, AFRL/VAAC, 2210 Eighth Street. Associate Fellow AIAA.
†Associate Professor, Department of Engineering Physics, AFIT/ENP, 2950 P Street.

Introduction

THE problem of accurate modeling of hypersonic flow physics in aerospace applications has been the subject of several studies in the last decade, each attempting to reveal and address the difficulties of modeling the relaxation phenomena of the internal energy modes with widely separated timescales and the resulting thermal and chemical nonequilibrium.[1] The relatively slowly varying vibrational relaxation and dissociation mechanisms are coupled, only exacerbating the problem of defining a physically meaningful theoretical model amenable to numerical modeling for today's computational codes.

Dissociation may occur via different mechanisms in vibrationally excited flows.[2] In general, a diatomic molecule can undergo thermal dissociation if its internal energy exceeds the dissociation energy. The internal energy is the sum of the rotational, vibrational, and electronic energies. Dissociation may occur from the ground electronic and vibrational state due to rotational excitation, when the rotational energy is much higher than the dissociation energy. Dissociation of a nonrotating molecule can occur from the electronic ground state due to molecular vibrations and a nonrotating, nonvibrating molecule in a transition from the electronic ground state to a repulsive excited electronic state. Here also the energy of the state is considerably higher than the dissociation energy. In the standard ladder model of dissociation, molecules are excited to higher and higher vibrational states and dissociate by making a transition to the continuum. In this model, the rotational structure is neglected. To implement one or more of the mentioned dissociation mechanisms, a state kinetic approach where the state-to-state transitions are modeled becomes attractive and may even be necessary to gain some insight in to the flow physics. Some recent attempts[3–6] to couple the vibrational master equation with state-to-state kinetics to the

fluid dynamic equations are encouraging and offer new possibilities for research in nonequilibrium flows.

The validity of the numerical simulation of nonequilibirum flows critically depends on the relaxation times used for modeling energy transfer among the various internal energy modes. Experiments on shock-standoff distance to determine the relaxation time of the nonequilibrium modes were discussed in Ref. 7. Although the oxygen vibrational relaxation times proposed by different authors agree well within experimental uncertainty, the dissociation rates at high temperatures differ by more than a factor of 10 (Ref. 8). A widely used empirical model of nonequilibrium vibration–dissociation coupling to date is the one attributed to Park.[1,9,10] The model weighted more toward the vibrational temperature due to the preferential dissociation concept which matched experimental data for radiative energy flux.[10] Park proposed an effective temperature for the dissociation with the form $T_{\text{eff}} = T^m T_{\text{vib}}^{1-m}$. Typically, values of the exponent range from $0.5 \leq m \leq 0.7$. Although the model lacks a sound physical justification, it does reproduce some of the slower observed dissociation rates. The model, however, does not reproduce experimental vibrational temperature data[11] and underpredicts shock-standoff distance for a series of calculations below Mach 12, which encompass vibrationally excited and dissociating flows.[12,13] These calculations clearly reveal the need to model the vibration–dissociation coupling taking into account one or more fundamental mechanisms controlling the dissociation process at the quantum level.

A number of studies[14,15] attempted to provide a physical basis to the vibration–dissociation coupling. However, these studies were successful only to the extent of showing the inadequacy of the Park's model.[10] Osipov and Stupochenko[2] in their study of the kinetics of thermal dissociation show that the vibrational population distribution function is altered by the dissociation process. As equilibrium is approached, a quasi-steady state is achieved, and the populations obtain a self-similar form. The dissociation losses from the vibrational manifold tend to reduce the vibrational populations below their equilibrium values, resulting in the lowering of the dissociation rate. At equilibrium, the net loss due to dissociation and recombination is zero, and there is no depletion of the population; the present study assumes under these conditions that the rate of dissociation is given by Park with $T = T_v$. It is convenient to divide the vibrational relaxation in to two *time* regimes. Initially, over a time $\tau_{\text{V-T}}$ a quasi-steady distribution is established. Over a much longer time τ_{diss}, this distribution approaches the equilibrium distribution, and the atoms and molecular species concentrations then ultimately satisfy the law of mass action. Here we consider the evolution of the quasi-steady distribution as it evolves in time toward the equilibrium distribution. With $\tau_{\text{V-T}} < t \leq \tau_{\text{diss}}$, two opposing factors, characterize this state: vibrational–transtational (V–T) trying to establish equilibrium and dissociation disrupting and perturbing the distribution. To simplify the analysis in the present study, dissociation is restricted to the last discrete vibrational level. Figure 1 shows the exchange of energy in the vibrational mode and the eventual loss of vibrational quanta due to dissociation. Two types of models were implemented in the present work for studying the effect of vibrational relaxation and dissociation coupling on the flow physics. One is a lumped

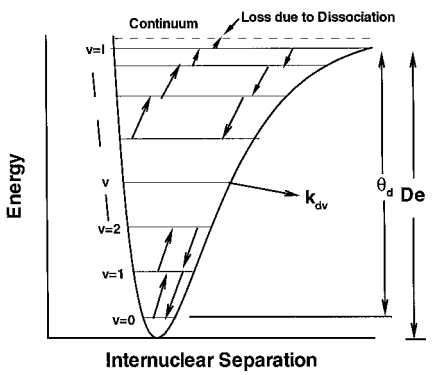

Fig. 1 Energy transitions of vibrational excitation and dissociation in a molecule.

Landau–Teller vibrational relaxation model[16] (LLTR) and the other is a discrete state kinetic relaxation model (DSKR). The LLTR is based on the assumption that the molecule behaves like a harmonic oscillator and the V–T transitions are approximated by the Landau–Teller theory. The DSKR model, applied to nitrogen in the present study views the molecule as anharmonic oscillator of 45 quantum levels, the kinetics of the particle exchanges among the quantum states is simulated by the vibrational master equation, and the populations are calculated assuming single quantum transitions.

The present study also addresses the effects of viscosity, thermal conductivity, and mass diffusion in the DSKR model and compares this prediction with the more popular LLTR model for flows in small departures from equilibrium. Code validation is performed with experimental shock standoff distances[17] obtained in the ballistic range and also by comparing present results with results from two other computational codes[12,18] having similar physical modeling as the present work. As a means to address the inadequacy[13] of the Park's two-temperature model,[10] dissociation rates predicted by the present master-equation-based vibration–dissociation coupling model are used to simulate nitrogen flow at Mach 19.83 past a 0.1524-m-radius body at 60-km altitude conditions.

Analysis

This section gives the governing equations used for coupling to the LLTR and DSKR.

The global conservation equations in mass-averaged velocity form are

$$\frac{\partial}{\partial t}(\rho_v) + \nabla \cdot \left[\rho_v\left(\boldsymbol{u} + \boldsymbol{u}_{\text{N}_2} + \boldsymbol{u}_{v\text{N}_2}\right)\right] = \dot{\omega}_v \qquad v = 0, 1, \ldots \tag{1}$$

$$\frac{\partial}{\partial t}(\rho_s) + \nabla \cdot [\rho_s(\boldsymbol{u} + \boldsymbol{u}_s)] = \dot{\omega}_s \tag{2}$$

$$\frac{\partial}{\partial t}(\rho \boldsymbol{u}) + \nabla \cdot (\rho \boldsymbol{u}\boldsymbol{u} + \tilde{\tau}) = 0 \tag{3}$$

$$\frac{\partial}{\partial t}(\rho e_{\text{vib}}) + \nabla \cdot [\rho e_{\text{vib}}(\boldsymbol{u} + \boldsymbol{u}_s) + \dot{q}_{\text{vib}}] = \rho \dot{\omega}_{\text{vib}} + e_{\text{vib}}\dot{\omega} + Q_{\text{V-T}} \tag{4}$$

$$\frac{\partial}{\partial t}(\rho e) + \nabla \cdot \left[\rho\left(e + \frac{p}{\rho}\right)\boldsymbol{u} - \left(\sum \dot{\boldsymbol{q}}_{\text{vib}} + \dot{\boldsymbol{q}}_{\text{trans}}\right) + \sum(\rho_s h_s \boldsymbol{u}_s) - \boldsymbol{u} \cdot \tilde{\tau}\right] = 0 \tag{5}$$

The conservation equation (1) used in the DSKR code is written for mass density in quantum level v for diatomic nitrogen. The term $\boldsymbol{u}_{\text{N}_2}$ is the diffusion velocity of component N_2 of the gas mixture, and $\boldsymbol{u}_{v\text{N}_2}$ is the diffusion velocity of level v relative to N_2 diffusion velocity. The source term $\dot{\omega}_v$ derived from the vibrational master equations is made up of the relevant energy exchange processes consisting of the V–T and vibrational–vibrational (V–V) reaction mechanisms. Of the three species (O_2, N_2, and O) considered for the air mixture in the DSKR code, only the species N_2 was treated as an anharmonic oscillator in the DSKR model with the following energy exchange mechanisms:

$$\dot{\omega}_v = \left(\dot{\rho}_{\text{N}_2-\text{N}_2}\right)^{\text{V-T}} + \left(\dot{\rho}_{\text{N}_2-\text{N}_2}\right)^{\text{V-V}} + \left(\dot{\rho}_{\text{N}_2-\text{O}_2}\right)^{\text{V-T}} + \left(\dot{\rho}_{\text{N}_2-\text{O}}\right)^{\text{V-T}} + \left(\dot{\rho}_{\text{N}_2\to\text{N}}\right)^{\text{diss}} + \left(\dot{\rho}_{\text{N}\to\text{N}_2}\right)^{\text{recomb}} \tag{6}$$

The density of molecular nitrogen is the sum of population densities in the various vibrational levels:

$$\rho_{\text{N}_2} = \sum_{v=0,1,\ldots} \rho_v \tag{7}$$

The mass conservation of species treated in the LLTR model is represented by Eq. (2). The production of small amounts of atoms due to dissociation of molecules is included in the source term $\dot{\omega}_s$. The term $\boldsymbol{u}_s$ is the diffusion velocity of component s of the gas mixture. The mixture density ρ is the sum of the partial species densities,

$$\rho = \rho_{N_2} + \rho_{O_2} + \rho_O + \rho_{NO} + \rho_N \tag{8}$$

For simulations in air, the maximum temperature of the shock was below 7000 K, thereby necessitating the oxygen dissociation reaction in the DSKR code. Because of the small amount of nitrogen dissociation and the difficulty of incorporating collision probabilities of additional species, only oxygen dissociation was considered in the DSKR model. However, the LLTR code considered N and NO also.

Equation (3) gives the conservation of total momentum. Equation (4) is the conservation equation for vibrational energy where Q_{V-T} denotes the energy exchange between the vibrational and translational modes. For diatomic nitrogen in the DSKR code, a separate vibrational conservation equation was not necessary because the vibrational energy was calculated at each quantum level, discussed later. The diatomic oxygen molecules in the DSKR code and all of the species in the LLTR model were assumed as harmonic oscillators. Equation (4) was solved with a source term for the V–T coupling, modeled according to the Landau–Teller[16] (see also Ref. 19) form:

$$\dot{\omega}_{vib} = \left(e^*_{vib_s} - e_{vib_s}\right)\Big/\tau_s \tag{9}$$

where e_{vib_s} is the vibrational energy of the molecular species s, $e^*_{vib_s}$ is the vibrational energy in thermal equilibrium at the local translational temperature, and the relaxation time is given by

$$\tau_s = \frac{\sum_s X_s}{\sum_s X_s/\tau_{LT}} \tag{10}$$

where X_s is the species mole fraction and τ_{LT} is the Landau–Teller[16] interspecies relaxation times. Here τ_{LT} was computed using the expression developed by Millikan and White.[20] The vibrational temperature of molecular species s was determined by inverting the expression for the vibrational energy contained in a harmonic oscillator at the temperature T_v,

$$e_{vib(s)} = R\Theta_{v(s)}\Big/\left\{\exp\left[\Theta_{v(s)/T_v}\right] - 1\right\} \tag{11}$$

where R is the species gas constant per unit mass. V–V exchanges were considered only between the nitrogen molecules in the DSKR model used to compare to the LLTR model; they were neglected for the oxygen molecules in the DSKR model and all of the species in the LLTR model. The DSKR model incorporating the new vibration–dissociation coupling neglected V–V exchanges also. Equation (4) also includes terms for the conduction and diffusion of vibrational energy. The conservation of total energy is given by Eq. (5) with heat conduction and species diffusion terms.

The kinetics of the particle exchanges among the quantum states of N_2 were simulated by the vibrational master equations. The population distributions were calculated by[6]

$$\dot{\omega}_v = \frac{1}{M}\Bigg\{\sum_{v'}[k_{V-T}(v' \to v)\rho_{v'}\rho - k_{V-T}(v \to v')\rho_v\rho] + \sum_w [k_{V-V}(v', w' \to v, w)\rho_{v'}\rho_{w'} - k_{V-V}(v, w \to v', w')\rho_v\rho_w]\Bigg\} \tag{12}$$

where only single quantum transitions have been considered. The equations governing the V–T reactions responsible for the variation of the particles distributed in the vth vibrational level of diatomic nitrogen are

$$N_2(v) + M \rightleftharpoons N_2(v-1) + M \tag{13}$$

where M represents O_2, O, and N_2. The equations governing the V–V processes in N_2 giving the reactions responsible for the variation of the particles distributed in the vth vibrational level are

$$N_2(v) + N_2(w) \rightleftharpoons N_2(v-1) + N_2(w+1) \tag{14}$$

For the kinetics of diatomic nitrogen, the present study used 1) V–T forward rate coefficients calculated according to expressions proposed by Capitelli et al.[21] and Billing and Fisher[22] and 2) V–V forward rates by Doroshenko et al.[23] The V–T forward rate coefficient for N_2–O collisions was from the work of Capitelli et al.,[4] which was based on Refs. 24 and 25. Reverse rate coefficients were derived from detailed balance.

In the present study, for the N_2–O_2 collisions, the Landau–Teller theory was used to determine the V–T relaxation time[16] τ_{LT} from Millikan and White correlations.[20] The forward $k_{v-1,v}$ rates were scaled from the rate constants $k_{1,0}$ (Ref. 19), and the reverse $k_{v,v-1}$ rates were scaled from detailed balance. Expressions for the rate constant, forward and backward rates are

$$k_{1,0} = 1/\tau_{LT}[1 - \exp(-\Theta_v/T)] \tag{15}$$

$$k_{v-1,v} = vk_{1,0}\exp(-\Theta_v/T) \tag{16}$$

$$k_{v,v-1} = vk_{1,0} \tag{17}$$

The vibrational energy of the N_2 molecule is given in terms of the quantum level energies by

$$e_{vib_{N_2}} = \sum_{i=1,2,\ldots} \frac{\rho_i}{\rho_{N_2}}\epsilon_i \tag{18}$$

where the index i is used to denote the quantum level. In this equation, ρ_i/ρ_{N_2} is the fractional population of the ith vibrational level, and ϵ_i the quantum level energy given by the third-order approximating formula

$$\epsilon_i/hc = \omega_e\left(i - \tfrac{1}{2}\right) - \omega_e x_e\left(i - \tfrac{1}{2}\right)^2 + \omega_e y_e\left(i - \tfrac{1}{2}\right)^3 \qquad i = 1, 2, \ldots, l+1 \tag{19}$$

Equation (19) represents anharmonic-oscillator behavior of the N_2 molecule, where h is Planck's constant and c is the speed of light. The spectroscopic constants are given by[26] $\omega_e = 2358.57$ cm^{-1}, $\omega_e x_e = 14.324$ cm^{-1}, and $\omega_e y_e = -0.00226$ cm^{-1}. When $i = 45$, the value of energy exceeds the N_2 dissociation energy 9.62 eV (Ref. 27).

The primary species of air considered in the DSKR code were O_2, O, and N_2. For the maximum shock temperature of 7000 K, the significant chemical reaction between the species considered are

$$O_2 + M \rightleftharpoons 2O + M \tag{20}$$

The LLTR code considered, in addition, nitrogen dissociation and nitric oxide formation, which is expected to be small at the temperatures considered in this study. For the Mach 19.83 case of a pure nitrogen medium, the maximum shock temperature was 20,000 K, and the dissociation reaction for the nitrogen molecule considered was

$$N_2 + M \rightleftharpoons 2N + M \tag{21}$$

The chemical source terms were derived from the law of mass action. The reaction rates and equilibrium constants were taken from the work of Park.[9] The vibration–dissociation coupling for the diatomic species was achieved by the two-temperature model suggested by Park[9]: $T_{eff} = \sqrt{(TTv)}$, where T_{eff} is the rate-controlling temperature for the forward rate of the dissociation–recombination reactions. In addition, Park's rates from Refs. 10 and 28 and Oertel's oxygen dissociation rates[8] were also used for comparison to the Park's rates from Ref. 9. See the Appendix Tables A1–A6 for a tabulation of the rates used and Fig. 2 for the variation of the forward rate coefficients of oxygen dissociation with temperature up to 10,000 K. Note that Oertel's oxygen dissociation rates[8] are dependent on translational temperature alone unlike Park's rates. The DSKR-based vibration–dissociation coupling model predicted new set of rates for nitrogen dissociation, which account for depletion effects in the vibrational population.

Transport Effects

In the present LLTR code, the species viscosity was computed from the curve fits of Blottner et al.[29] and the species thermal

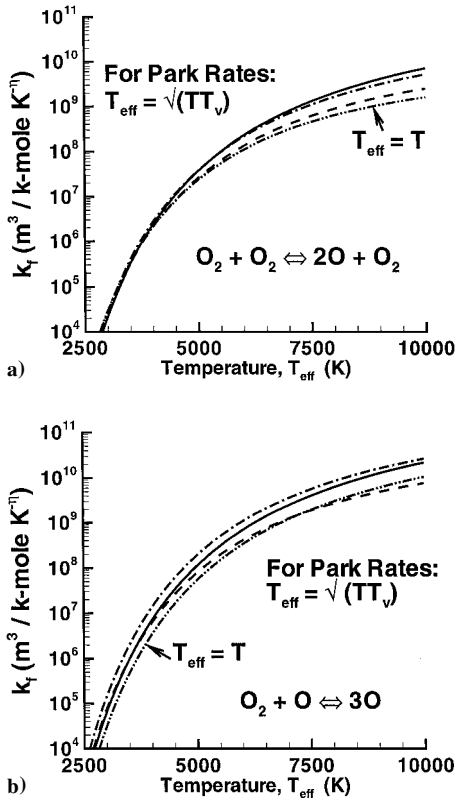

Fig. 2 Rate coefficients of oxygen dissociation reaction with O_2 and O as partners: ——, Park (Ref. 9); – – –, Park (Ref. 10); –·–, Park (Ref. 28); and –···–, Oertel (Ref. 8).

conductivity from Eucken's relation (see Ref. 19). The viscosity and thermal conductivity of the mixture were computed by the Wilke's semi-empirical mixing rule (see Ref. 19). In the present analysis, only ordinary diffusion generated by species concentration gradients was considered, the diffusion mass flux calculated according to Fick's first law of diffusion (see Ref. 30). The binary diffusion coefficient in the Fick's law was calculated assuming a constant Lewis number of 1.4.

In the DSKR code, the mass diffusion terms in Eq. (1) were derived assuming Fick's law is valid (see Ref. 5),

$$\rho_{N_2} \boldsymbol{u}_{N_2} = -\rho D_{12} \nabla \left(\rho_{N_2} / \rho \right) \tag{22}$$

$$\rho_{N_2} \boldsymbol{u}_{vN_2} = -\rho_{N_2} D_{11} \nabla \left(\rho_{vN_2} / \rho_{N_2} \right) \tag{23}$$

The coefficients D_{11} and D_{12} are the self- and binary-diffusion coefficients, respectively. The binary diffusion coefficient was obtained by assuming a constant Lewis number for both species. The self-diffusion coefficient was given by

$$D_{11} = \eta \mu_{N_2} / \rho \tag{24}$$

where η is the effective Lewis number of 1.2 (Ref. 31).

Vibration–Dissociation Coupling

This section presents the kinetic equations describing the dissociative-relaxation coupling considering the balance equations for the numbers of particles in each vibrational level[2]:

$$\dot{\rho}_v = \sum_{v'} \left[k_{V-T}(v' \to v) \rho_{v'} \rho_{N_2} - k_{V-T}(v \to v') \rho_v \rho_{N_2} \right] + k_{rv} \rho_N^2 \rho_{N_2} - k_{dv} \rho_v \rho_{N_2} \qquad v = 0, 1, \ldots, l \tag{25}$$

$$\frac{1}{2} \dot{\rho}_N = \sum_{v=0}^{l} k_{dv} \rho_v \rho_{N_2} - \sum_{v=0}^{l} k_{rv} \rho_N^2 \rho_{N_2} \tag{26}$$

where ρ_v is the mass density in level v, $k_{v' \to v}$ and $k_{v \to v'}$ are the V–T rate coefficients for vibrational transitions to occur from $v' \to v$ and $v \to v'$, and k_{dv} and k_{rv} are the rate constants for dissociation/recombination in transition from/to vibrational state v to/from continuum. Also ρ_N is the density of nitrogen atoms resulting from dissociation, and ρ_{N_2} is the number of colliding molecules. Here l is the last discrete vibrational level of the molecule. Note that

$$\sum_{v=0}^{l} \rho_v = \rho_{N_2}$$

If we can define φ_v to give the deviation of the quasi-steady distribution from an equilibrium Boltzmann distribution, then the mass density in vibrational state v is

$$\rho_v(t) = \rho_v^{(0)} (1 + \varphi_v) \tag{27}$$

The deviation of the population of level v from equilibrium is given by φ_v, which relates ρ_v (the state mass density in level v) to $\rho_v^{(0)}$ (the state mass density in level v at equilibrium). It is seen that, when $\varphi_v < 0$, the level population decreases relative to the equilibrium population. The deviation coefficient φ_v in the simplest case of single-quantum energy transitions and dissociation only from the last discrete vibrational level is given by

$$\varphi_v = \frac{\dot{N}_2}{\rho_N \rho_{N_2}} \sum_{i=1}^{v} \frac{1}{k_{i-1,i} \Gamma_{i-1}} \left(\sum_{j=0}^{i-1} \Gamma_j \right) + \varphi_0 \tag{28}$$

where $\dot{N}_2$ is the global rate of the dissociation reaction. The unknown φ_0 term that gives the deviation for the first discrete vibrational level is determined from the normalization condition for Eq. (27) given by

$$\sum_{v=0}^{l} \rho_v^{(0)} \varphi_v = 0$$

From this condition, it follows that

$$-\varphi_0 = \frac{1}{\rho_{N_2}} \sum_{v=1}^{l} \rho_v^{(0)} \tilde{\varphi}_v \tag{29}$$

where $\tilde{\varphi}_v = \varphi_v - \varphi_0$. The Γ_v term is given by

$$\Gamma_v = \frac{\exp(-\epsilon_v / kT)}{\sum_{v=0}^{l} \exp(-\epsilon_{v'} / kT)} \tag{30}$$

Conditions of Numerical Simulation

Numerical simulations were conducted for a Mach 8.6 and 11.18 case with both LLTR code and DSKR code for comparing shock-standoff distance with experimental data and studying the effect of diffusion flux in the DSKR code. The LLTR code further simulated conditions of Mach 11.18 case for three sets of Park's two-temperature model rates[9,10,28] and Oertel's rates[8] for oxygen dissociation based on translational temperature to study the variation, if any, in the shock-standoff distance. See the Appendix for a tabulation of the rates used and Fig. 2 for the variation of the forward rate coefficients of oxygen dissociation with temperature up to 10,000 K. An earlier[32] Mach 7.7 computaton using LLTR model is also presented in the shock-standoff comparisons for reference purpose.

Details of rates used for vibrational energy transfer the two codes used in this study of given in Table 1.

Table 1 Details of rates used for vibrational energy transfer DSKR and LLTR codes

No.	Code	Species	Oscillator	Collides with	V–T rates	V–V rates
1	DSKR	N_2	Anharmonic	N_2	Ref. 21	Ref. 23
2	DSKR	N_2	Anharmonic	O_2	Ref. 20	——
3	DSKR	N_2	Anharmonic	O	Ref. 4	——
4	DSKR	O_2	Harmonic	N_2, O	Ref. 20	——
5[a]	LLTR	S-species air	Harmonic	S-species air	Ref. 20	——

[a]For testing vibration–dissociation coupling DSKR-based V–T rates for N_2 used for Mach 19.8 case (see Table 2).

Table 2 Details of flow conditions in freestream

Case no.	Code	Mach no.	Freestream velocity, m/s	T_∞, K	$T_{v\infty}$, K	p_∞, Pa	Radius, m	Medium	Validation
1	LLTR	7.7	2630	293	293	600	0.014	Air	Exp[16]
2	DSKR and LLTR	8.6	2930	293	293	560	0.015	Air	Exp[16]
3	DSKR and LLTR	11.18	3844	293	293	1200	0.007	Air	Exp[16]/computation[12,17]
4[a]	LLTR	19.83	7000	300	300	27	0.1524	N_2	Computation[15]

[a]Includes new DSKR-based dissociation rates.

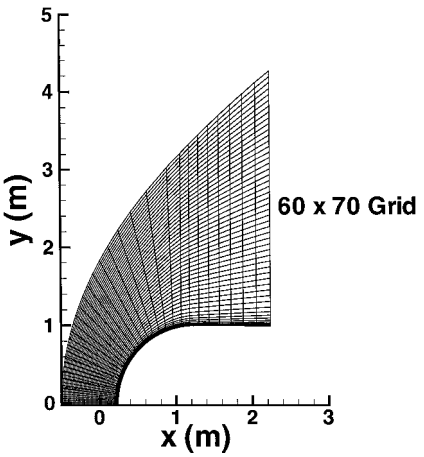

Fig. 3 Typical computational grid.

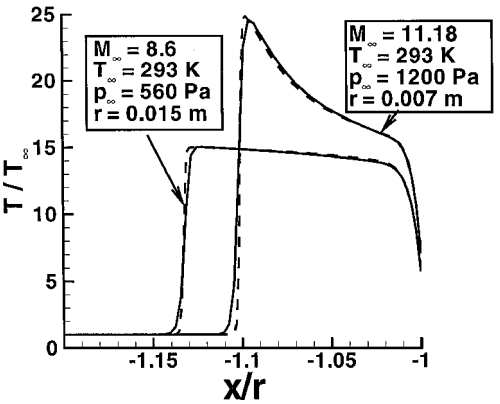

Fig. 4 Temperatures along the stagnation streamline, in air: ——, viscous (DSKR for N_2), and – – –, viscous (LLTR).

The DSKR model predicted new dissociation rates that were compared to the Park's two-temperature rates of Ref. 9. These new rates were implemented in a Mach 19.93 pure nitrogen flow past a blunt body and the shock-standoff distance was compared with a simulation that used the Park's two-temperature rates.[9] A summary of these cases is given in Table 2. Results predicted by the NASA code LAURA.4.7.1 (Ref. 17) were used for validation of the Mach 11.18 case. The physical models of LAURA code are described in Ref. 33.

The numerical algorithm employed to solve the coupled set of equations is the Roe flux difference method with entropy correction used in Ref. 6. An explicit predictor–corrector method is used to advance the solution in time. A grid size study was conducted to determine the effects of grid density on the temperature distribution along the stagnation streamline and surface. A mesh system of 60 nodes in the body-tangential direction and 70 nodes in the body-normal direction was used for all of the cases in the present study. The minimum distance Δ_n/r of the first mesh point away from the body was 0.0012, and the grid was exponentially stretched in the body-normal direction with a stretch factor of 1.27. A typical grid system of a hemisphere cylinder used for the axisymmetric computations presented in the present study is shown in Fig. 3.

Convergence to a steady-state solution was monitored by the L_2 norm. The data processing rate (DPR) of the air code with three species for the axisymmetric solution of the viscous equations coupled to the DSKR model with 45 quantum levels is 7.05×10^{-4} CPU seconds per point per iteration on a single processor of a Cray T-90 computer. The DPR of the air code with five species for the axisymmetric solution of the viscous equations coupled to the LLTR model is 1.13×10^{-4} CPU seconds per point per iteration on a single processor of a Cray T-90 computer.

Boundary Conditions

The upstream and far-field boundary conditions were prescribed as the undisturbed freestream values. At the downstream boundary, the no-change condition was imposed for the predominantly supersonic flowfield. On the body surface, $\boldsymbol{n} \cdot \boldsymbol{u}$ is zero, where $\boldsymbol{n}$ is the surface normal vector. The body surface is assumed to be noncatalytic. The finite volume formulation of the present work allows fluxes at the singular line of symmetry to be set to zero because the control surface of the elementary cell at the axis of symmetry merges to a point.

In the DSKR model code, the population densities in N_2 were set to values corresponding to a Boltzmann distribution at the temperature $T_{v\infty}$ on the first i levels of the spectrum produced by Eq. (19). Thus, $\rho_{i,\infty}$ is given by

$$\frac{\rho_{i,\infty}}{\rho_{N_2\infty}} = \frac{\exp(-\epsilon_i/kT_v)}{\sum_{j=1,2,\ldots} \exp(-\epsilon_j/kT_v)} \qquad i = 1, \ldots, l \qquad (31)$$

where k is the Boltzmann constant. Vibrational temperature T_v in the freestream is in equilibrium with translational temperature. See Table 2 for a summary of flow conditions used in the present study. Initial conditions were set to freestream uniform flow conditions.

Results and Discussion

Results are presented in three sections. The first section compares results from the LLTR and the DSKR models with viscous effects. The second section presents results on validation of flowfield prediction using a LLTR model. The third section presents results of the new DSKR-based vibration–dissociation coupling model and simulation results of the Mach 19.83 case computed with the new dissociation rates and the rates[9] of a Park's two-temperature dissociating model.[10]

Comparison of LLTR and DSKR Models with Viscous Effects

Results of the DSKR inviscid and viscous codes are compared to the LLTR-based viscous code. Mach numbers of 8.6 and 11.18 were considered in airflow past 0.015- and 0.007-m-radius bodies, respectively. See Table 2 for more details on the flow conditions.

Figure 4 shows the translational temperatures along the stagnation streamline for Mach 8.6 and 11.18 flows. The flow is very close to $\gamma = \frac{7}{5}$ flow conditions for the Mach 8.6 flow, but the higher Mach number case displays greater thermal and chemical nonequilibrium. Prediction by LLTR and DSKR models with different vibrational rate data are close to each other. The inclusion of diffusion flux in the DSKR model code does not result in a significant modification of the flowfield. Comparison of heat transfer on the surface in Fig. 5 shows the heat transfer prediction of both viscous codes within 5% attributable to the inclusion of nitrogen dissociation and nitric oxide formation only in the LLTR code, not in the DSKR code.

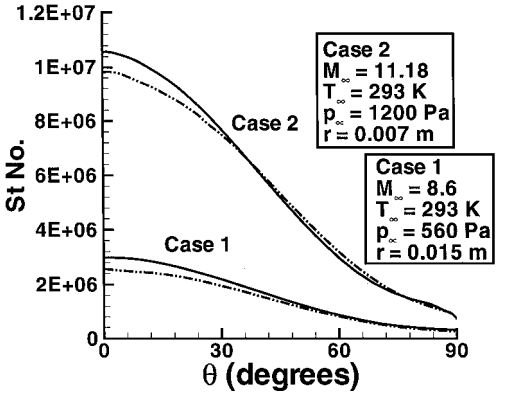

Fig. 5 Stanton number along surface, in air: ····, viscous (LLTR), and ——, viscous (DSKR for N_2).

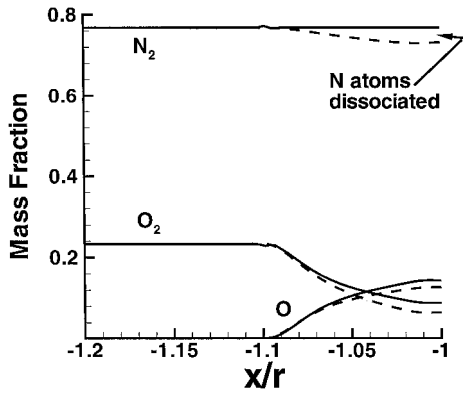

Fig. 6 Mass fraction along the stagnation streamline, $M_\infty = 11.18$, $p_\infty = 1200$ Pa, $T_\infty = 293$ K, $r = 0.007$ m, in air: – – –, viscous (LLTR), and ——, viscous (DSKR for N_2).

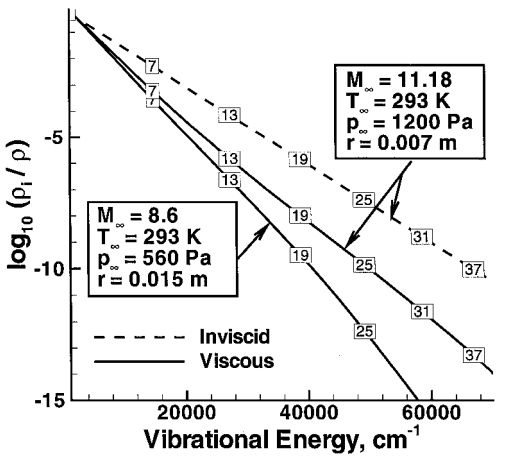

Fig. 7 N_2 population distribution at stagnation point.

The mass fraction for the Mach 8.6 case (figure not shown) has negligible dissociation at the maximum shock temperature of 4000 K. The mass fraction for Mach 11.18 case (Fig. 6) shows reduction in O_2 of 34% due to dissociation near the surface. The inclusion of nitrogen dissociation and nitric oxide formation in the LLTR model (not allowed in the DSKR model) causes a maximum difference of 10% in oxygen mass fraction between the models near the surface. The small amount (4%) of nitrogen dissociation can be seen from the N_2 variation near the surface from the LLTR model prediction. Nitrogen dissociation was not included in the DSKR model for this reason.

Figure 7 shows the nitrogen population distribution at the stagnation point. Here the viscous effects decrease the state density for the Mach 11.18 case. The lower Mach number case has a lower state density, but exhibits greater non-Boltzmann behavior at the upper levels because of lower temperature.

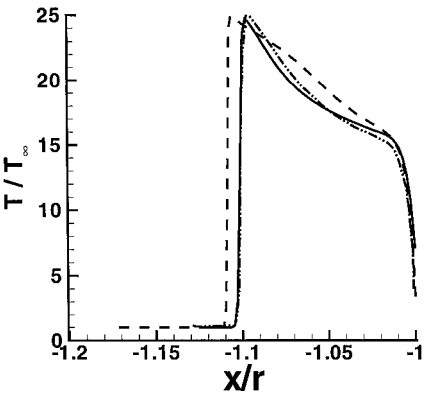

Fig. 8 Validation: temperatures along the stagnation streamline, $M_\infty = 11.18$, $p_\infty = 1200$ Pa, $T_\infty = 293$ K, $r = 0.007$ m, in air: – – –, Ref. 13 computation; ——, present computation; and ····, LAURA code computation.

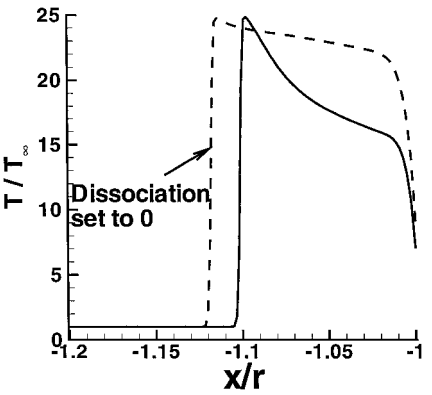

Fig. 9 Comparison of translational temperature along the stagnation streamline, $M_\infty = 11.18$, $p_\infty = 1200$ Pa, $T_\infty = 293$ K, $r = 0.007$ m, in air.

Validation

This section presents temperatures and shock-standoff distance comparisons of codes based on LLTR. Figure 8 shows computational prediction of translational temperature along the stagnation streamline of the present code with predictions of Ref. 12 and LAURA.[17] All codes are upwind difference type, and the physical models assume harmonic oscillator for vibrational relaxation and Park's $\sqrt{(TTv)}$ model[10] for dissociation. The prediction by the present code matches that of the LAURA code well. The prediction of Ref. 12, however, has a 7% higher shock-standoff distance and higher temperature in the shock layer.

The remainder of the results presented attempt to quantify the departure from idealized conditions and are variations of the present LLTR-based code. Figure 9 shows the translational temperature along the stagnation streamline compared with a computational prediction that included vibrational excitation but dissociation was set to zero. From Fig. 9 it is seen that the energy extracted by the dissociation process leads to a reduction of the shock-standoff distance by 14%. The influence of atomic recombination on the total energy is small, as seen in Fig. 10, where the present code with dissociation and recombination models is compared to a prediction that included dissociation, but recombination was set to zero.

A shock-standoff distance comparison, showing the deviation of experimental data and present computational predictions from idealized conditions, is provided in Fig. 11. For bodies flying at freestream velocities less than 3 km/s, the flow approximates frozen flow conditions, $\gamma = \frac{7}{5}$, where vibrational excitation is dominant but dissociation is negligible; the prediction of the present computation matches the experimental data point. At the higher freestream

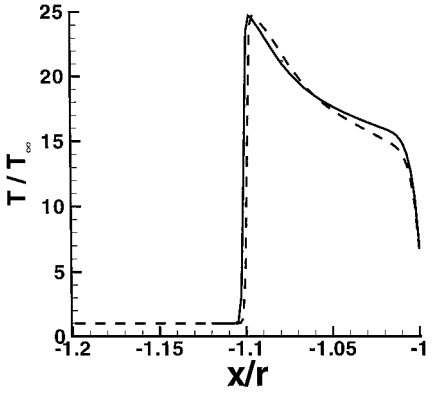

Fig. 10 Translational temperatures along the stagnation streamline showing effect of atomic recombination, $M_\infty = 11.18$, $p_\infty = 1200$ Pa, $T_\infty = 293$ K, $r = 0.007$ m, in air: ——, present, and – – –, recombination set to 0.

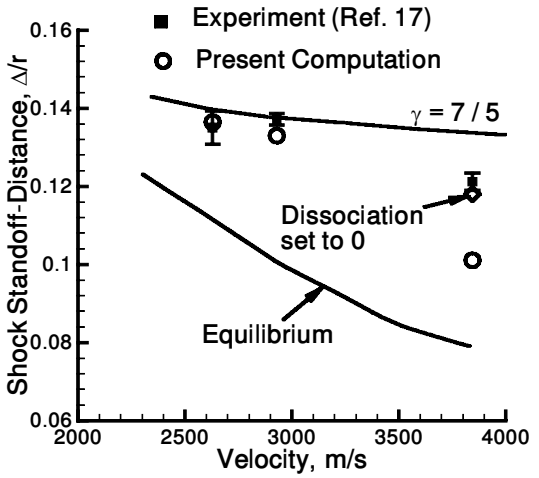

Fig. 11 Comparison of shock-standoff distances.

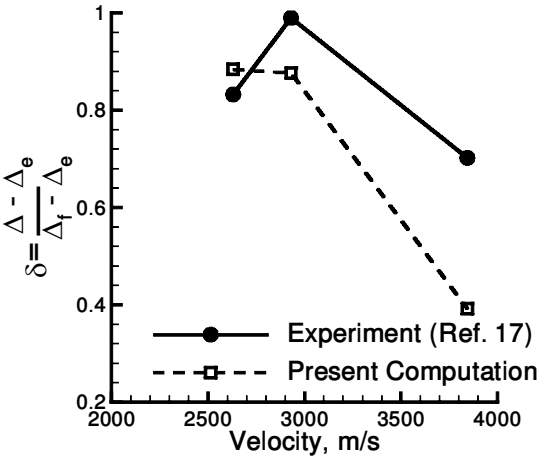

Fig. 12 Normalized shock stand-off distance parameter showing relative departure from equilibrium.

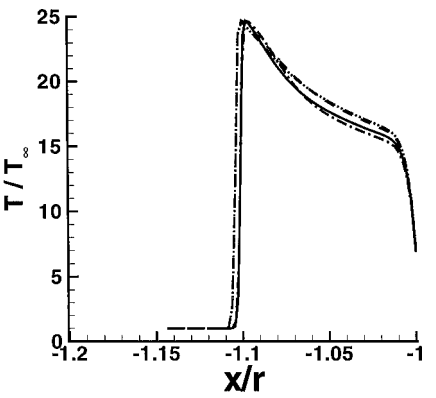

Fig. 13 Translational temperature along the stagnation streamline using different dissociation rates, $M_\infty = 11.18$, $p_\infty = 1200$ Pa, $T_\infty = 293$ K, $r = 0.007$ m, in air: ——, Park (Ref. 9); – – –, Park (Ref. 10); –·–, Park (Ref. 28); and –···–, Oertel (Ref. 8).

velocity, the Mach 11.18 case, the present code underpredicts the experiment[16] by 16%. For the same set of flow conditions, the computational predictions of Refs. 12 and 13 report a similar deviation from experiment. The present computation predicts 14% lower than the idealized case, where the dissociation was set to zero, 24% less than that at $\gamma = \frac{7}{5}$ and 20% higher than equilibrium conditions. However, the experimental data point is only 6% less than at $\gamma = \frac{7}{5}$. Clearly the dissociation rates of the Park $\sqrt{(TTv)}$ dissociating model[10] are high as noted also by Furudate et al. in Ref. 13. Because the present computation with the idealized case of dissociation set to 0 is about 2% less than the experimental data, the vibrational relaxation rates appear to be somewhat high also.

Figure 12 shows variation of a normalized parameter, $\delta = (\Delta - \Delta_e)/(\Delta_f - \Delta_e)$, the ratio of departure of shock-standoff distance from equilibrium to the difference in standoff corresponding to frozen and equilibrium conditions. The results are observed to lie approximately on a horizontal line[7] indicating that a fixed factor relates the disparate relaxation parameters to each other. The departure of the computation at 3844 m/s from the fixed factor is obvious from Fig. 12, signifying an incorrect prediction of one or more of the relaxation mechanisms. The experimental measurement at 2930 m/s also shows a small departure from the fixed factor.

Finally, the effect of different dissociation rates proposed by Park in Refs. 9, 10, and 28 and Oertel[8] (tabulated in the Appendix) are shown in Fig. 13. Because the translational temperature is about 7000 K, dissociation of oxygen will be more significant than nitrogen. See rate comparisons of oxygen dissociation shown earlier in Figs. 2a and 2b. Inspection of the forward reaction rates of $O_2 + O$ reaction reveals that the rates proposed in Ref. 28 are a maximum of four times faster than the rates of Ref. 10 at the highest temperature of 10,000 K. For the $O_2 + O$ reaction, rates of Ref. 9 are a maximum of five times faster than those of Oertel[8] at 10,000 K. Despite these differences, the shock-standoff distances vary less than 5%, and there is an underprediction of about 15% from the experimental data. Note that the rates proposed by Oertel[8] for oxygen dissociation based on translational temperature in the dissociation model predicts the same (Fig. 13) as Park's rates[10] based on the two-temperature model. It may be concluded that the Park two-temperature model and the associated dissociation rates are not adequate at these conditions and predict excessive dissociation resulting in incorrect shock-standoff distances, temperatures, and densities in the shock layer. Hence, a more physically meaningful model is required for the vibration–dissociation coupling for hypersonic flows about blunt bodies in the intermediate Mach number range.

Vibration–Dissociation Coupling

This section considers the new coupling model and presents the effects of dissociation on depletion of vibrational quanta in the N_2 molecule. The flowfield predictions by the new DSKR-based rates are compared with predictions by the Park's dissociation rates.[9]

Figure 14 shows the term in Eq. (27), $1 + \varphi_l$ and its inverse, which gives the dissociation reduction factor from Park's equilibrium rates plotted as a function of temperature. Note that when $\varphi_l < 0$, the effect is to deplete the population in the vibrational states. The reduction factor, $1/(1 + \varphi_l)$, is the ratio of the level population distribution at equilibrium to the nonequilibrium state. The reduction factor that accounts for the deviation from the quasi-steady-state distribution can range from 1 to 3 orders of magnitude between the temperatures of 5000–10,000 K at which there is considerable nitrogen dissociation. This factor was applied as a correction to the Park's dissociation rates

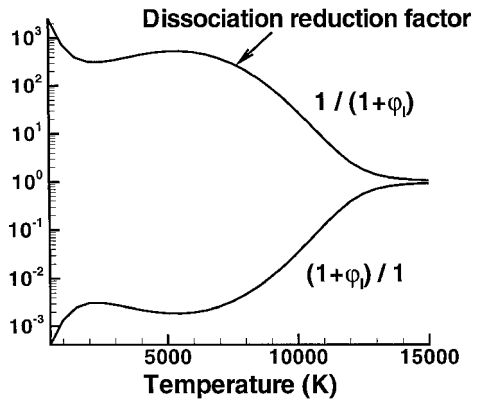

Fig. 14 Equilibrium and nonequilibrium population ratio and reduction factor for Park's dissociation model.

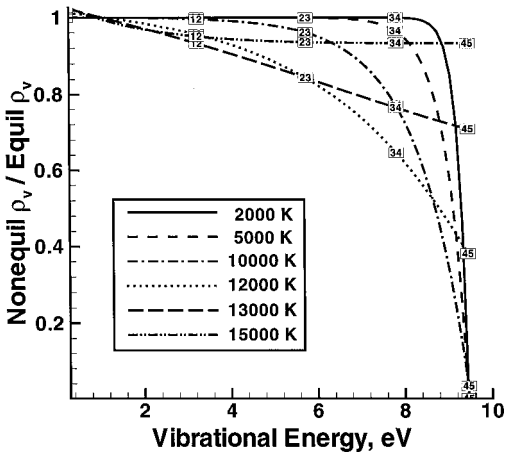

Fig. 15 Ratio of population distribution showing effect of depletion in quantum levels.

to account for the depletion effects in the vibrational levels. Note that the reduction factor is the highest below 2000 K, but there is negligible nitrogen dissociation at this temperature. The reduction factor again peaks at about 6000 K and stays high till 12,000 K, a region of significant nitrogen dissociation, and at higher temperatures begins to fall and reaches a factor of 1 at the highest temperature of 15,000 K shown in the Fig. 14. This behavior helps to explain the reason for the validity of Park's rates only in certain temperature ranges.

The depleted vibrational state populations in N_2 resulting from the ladder climbing dissociation model with the dissociation loss to the continuum restricted to the last discrete vibrational level are presented in Fig. 15. For clarity, the ratio of state density variation is shown only for certain representative temperatures. The population density shown as a factor of the equilibrium population undergoes a reduction in the excited vibrational states. The loss is significant in the upper levels shown for the low temperatures between 2000 and 5000 K. At higher temperatures, the depletion extends to lower levels also, as can be seen for 12,000 K, where the loss occurs in the level range of 6–45. Above 12,000 K, however, the reduction in the vibrational level population diminishes, and at the highest temperature of 15,000 K, the reduction is negligible. The varying loss in quantum level vibrational population at different temperatures was shown earlier in Fig. 14.

Figures 16–21 show results of computations of a Mach 19.83 case at 60-km altitude conditions for a nitrogen flow past a 0.1524-m-radius hemisphere cylinder with the new vibration–dissociation model and Park's $\sqrt{(TTv)}$ model. The ratio of the temperatures and forward dissociation rate coefficients as applied to the Park's two-temperature model[10] for the Mach 19.83 case is seen in Fig. 16. (Note that maximum shock temperature is 20,000 K, and the wall temperature is 300 K, shown in Fig. 17.) The ratio of T_v/T along the stagnation streamline is reduced by a maximum of 70% in a narrow region near the shock, but is nearly equal to 1 in most of the shock layer. Note that the present analysis considers the depletion effects governed by the translational temperature only. Thus, the reduction factor is applicable to the entire region of the shock layer except for the narrow region near the shock: In this narrow region, because the effective temperature is lower than the translational temperature, the depletion prediction in this study can be considered to be the effective maximum. Park's two-temperature

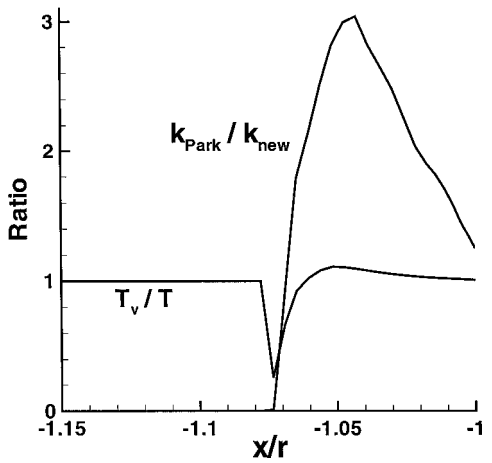

Fig. 16 Ratio of temperatures and dissociation rates along the stagnation streamline, $M_\infty = 19.83$, $p_\infty = 27$ Pa, $T_\infty = 300$ K, $r = 0.1524$ m, in N_2.

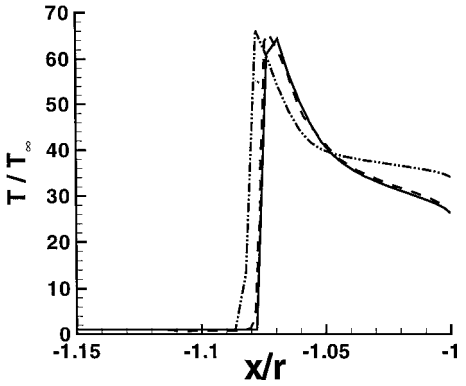

Fig. 17 Translational temperature along the stagnation streamline using reduction factor for Park's model, $M_\infty = 19.83$, $p_\infty = 27$ Pa, $T_\infty = 300$ K, $r = 0.1524$ m, in N_2: – – –, Ref. 15 (Park TTv model); ——, present (Park TTv model); and –···–, present (Park TTv model with depletion).

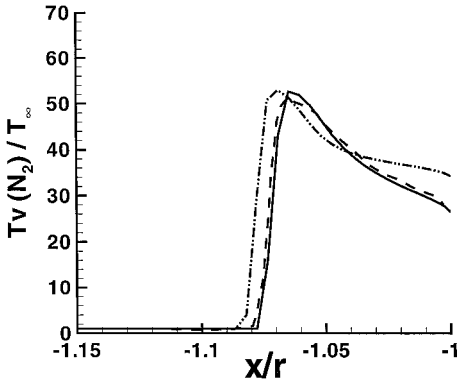

Fig. 18 Vibrational temperature along the stagnation streamline using reduction factor for Park's model, $M_\infty = 19.83$, $p_\infty = 27$ Pa, $T_\infty = 300$ K, $r = 0.1524$ m, in N_2: – – –, Ref. 15 (Park TTv model); ——, present (Park TTv model); and –···–, present (Park TTv model with depletion).

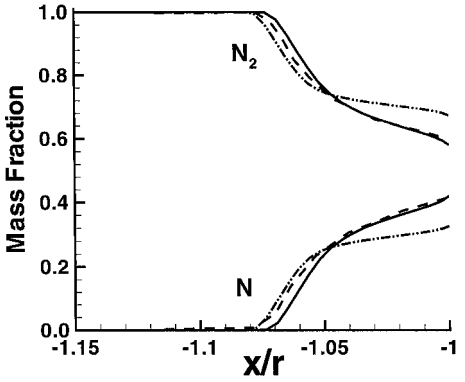

Fig. 19 Mass fraction along the stagnation streamline using reduction factor for Park's model, $M_\infty = 19.83$, $p_\infty = 27$ Pa, $T_\infty = 300$ K, $r = 0.1524$ m, in N_2: – – –, Ref. 15 (Park TTv model); ——, present (Park TTv model); and –···–, present (Park TTv model with depletion).

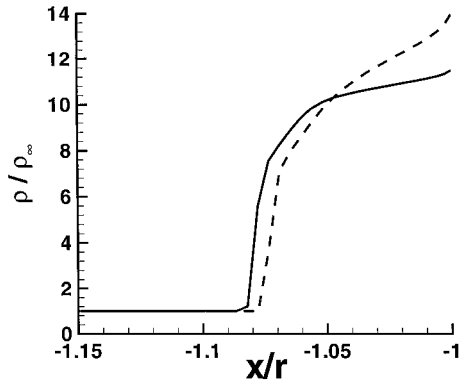

Fig. 20 Density along the stagnation streamline using reduction factor for Park's model, $M_\infty = 19.83$, $p_\infty = 27$ Pa, $T_\infty = 300$ K, $r = 0.1524$ m, in N_2: – – –, present (Park TTv model), and ——, present (Park TTv model with depletion).

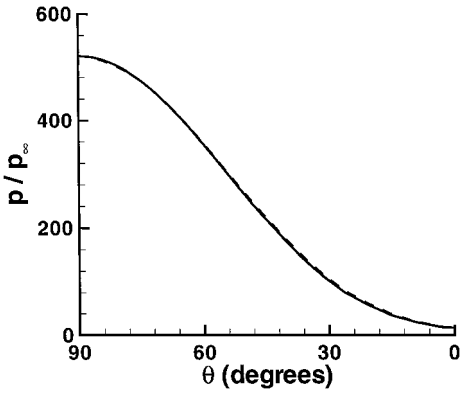

Fig. 21 Surface pressure using reduction factor for Park's model, $M_\infty = 19.83$, $p_\infty = 27$ Pa, $T_\infty = 300$ K, $r = 0.1524$ m, in N_2: ——, present (Park TTv model), and – – –, present (Park TTv model with depletion).

dissociation rates along the stagnation streamline peaked to a maximum of three times the new rates in the shock layer; the new rates result in a reduced endothermicity in the dissociation process. Near the surface, the effect of the new dissociation model for this set of flow conditions is negligible.

Figures 17–21 contrast the shock characteristics and flow conditions under the Park's $\sqrt{}$(TTv) dissociation model[10] and the new model. The two computational predictions (the present and that of Ref. 15) used for establishing a baseline with the Park's dissociation model match well. However, a significant effect is observed as an increase in shock-standoff distance compared to the Park's model by 8% and a higher shock-layer temperature near the surface (Figs. 17 and 18). The higher translational and vibrational temperatures between X/r of -1.0 and -1.5 are a result of the lower dissociation rates predicted by the new vibration–dissociation model. The temperatures are lower in the vicinity of the shock wave due to enhanced dissociation resulting from the ratio of $k_{\text{Park}}/k_{\text{new}} < 1$ (Fig. 16). The increase in shock-standoff distance is a result of reduced endothermicity of the new vibration–dissociation coupling model.

The corresponding mass fraction and density profiles are shown in Figs. 19 and 20. With the increase in shock-standoff distance predicted by the new model, a lowering of the density in the shock layer ($-1 \le X/r \le -1.04$) is seen; at the surface, the density is reduced by 17%. The surface pressure, however, does not show any difference between the two models (Fig. 21).

Concluding Remarks

A computational study was conducted of hypersonic flow past a hemisphere cylinder. Two types of models were used to study the effect of vibrational relaxation and dissociation coupling on the flow physics. One is an LLTR and the other is a DSKR. The viscous effects were included in both the computer codes of LLTR and DSKR. The DSKR code consisted of the vibrational master equations with 45 quantum energy levels of diatomic nitrogen, assumed as an anharmonic oscillator.

The simulated flow conditions, based on the availability of experimental data in the ballistic range, were primarily Mach numbers 8.6 and 11.18 at T_∞ of 293 K and p_∞ of 560 and 1200 Pa, respectively. Results predicted by the DSKR-based code were similar to those of the LLTR-based code for the Mach 8.6 and 11.18 cases. The shock-standoff distance prediction for the Mach 8.6 case matched the experiment. However, at Mach 11.18, the present computational results underpredicted the experimental shock-standoff distance by 16% due to high dissociation rates of the Park's two-temperature model.

A new DSKR-based vibration–dissociation model was studied. The new model considers depletion effects in the vibrational quantum levels of a molecule caused by dissociation loss to the continuum. The new model reduced the Park's equilibrium dissociation rates in the temperature range of 5000–15,000 K; in the lower temperature range, the reduction was substantial but the rates were consistent with Park's rates at the high end. Vibrational population depletion was observed mainly in the upper levels for $T < 5000$ K, but for $6000 < T < 12{,}000$ K, depletion occurred in the lower levels also. For $T > 13{,}000$ K, the depletion effects were negligible. The new model helps to explain the restricted success of Park's model and dissociation rates for certain temperature ranges in hypersonic flows. Application of the new model to a Mach 19.83 pure nitrogen flow predicted an 8% greater shock standoff distance due to lower dissociation rates compared to the standard Park's two-temperature model. Based on these findings, it expected that, by including the depletion effects in the vibration–dissociation coupling, the numerical simulations of the intermediate hypersonic airflows past a blunt body can be predicted with far greater accuracy.

Appendix: Tabulation of Reaction Rates Used

Table A1 Forward reaction rate coefficients, $k_f(T_{\text{eff}}) = C_f T_{\text{eff}}^{\eta} \exp(-\theta_{ds}/T_{\text{eff}})$, Park[9]

Reaction	M	C_f, $\text{m}^3/\text{kmole}\cdot\text{K}^{-\eta}$	η	Θ_{ds}, K
$N_2 + M \rightleftharpoons N + N + M$	N_2, O_2, NO	$3.7E{+}18$	-1.6	113,200
	N	$1.1E{+}19$	-1.6	113,200
	O	$1.1E{+}19$	-1.6	113,200
$O_2 + M \rightleftharpoons O + O + M$	N_2, O_2, NO	$2.75E{+}16$	-1.0	59,500
	N	$8.25E{+}19$	-1.0	59,500
	O	$8.25E{+}19$	-1.0	59,500
$NO + M \rightleftharpoons N + O + M$	N_2, O_2, NO	$2.3E{+}14$	0	75,500
	N	$4.6E{+}14$	-0.5	75,500
	O	$4.6E{+}14$	-0.5	75,500
$N_2 + O \rightleftharpoons NO + N$	—	$3.18E{+}10$	-0.1	37,700
$NO + O \rightleftharpoons O_2 + N$	—	$2.16E{+}09$	1.29	19,220

Table A2 Constants for computing equilibrium constants[a] used with dissociation rates[9] of Table A1[b]

Reaction	A_{1m}	A_{2m}	A_{3m}	A_{4m}	A_{5m}
$N_2 + M \rightleftharpoons N + N + M$	3.898	−12.611	0.683	−0.118	0.006
$O_2 + M \rightleftharpoons O + O + M$	1.335	−4.127	−0.616	0.093	−0.005
$NO + M \rightleftharpoons N + O + M$	1.549	−7.784	0.228	−0.043	0.002
$N_2 + O \rightleftharpoons NO + N$	2.349	−4.828	0.455	−0.075	0.004
$NO + O \rightleftharpoons O_2 + N$	0.215	−3.652	0.843	−0.136	0.007

[a]Equilibrium constants for the chemical reactions computed using $K_{eq} = \exp(A_{1m} + A_{2m}Z + A_{3m}Z^2 + A_{4m}Z^3 + A_{5m}Z^4)$, where $Z = 10,000/T$ (T is translational temperature in Kelvin).
[b]Here $k_b(T_{eff}) = k_f(T_{eff})/K_{eq}(T_{eff})$; K_{eq} units for the dissociation reactions are kmole/m^3 and the exchange reactions are dimensionless.

Table A3 Forward reaction rate coefficients, $k_f(T_{eff}) = C_f T_{eff}^{\eta} \exp(-\theta_{ds}/T_{eff})$, Park[10]

Reaction	M	C_f, m^3/kmole · K$^{-\eta}$	η	Θ_{ds}, K
$N_2 + M \rightleftharpoons N + N + M$	N_2, O_2	3.0E+18	−1.6	113,200
	NO	4.98E+18	−1.6	113,200
	N	1.6E+19	−1.6	113,200
	O	4.98E+19	−1.6	113,200
$O_2 + M \rightleftharpoons O + O + M$	N_2, O_2, NO	9.68E+19	−2	59,500
	N	2.9E+20	−2	59,500
	O	2.9E+20	−2	59,500
$NO + M \rightleftharpoons N + O + M$	N_2, O_2, NO	7.95E+20	−2	75,500
	N	7.95E+20	−2	75,500
	O	7.95E+20	−2	75,500
$N_2 + O \rightleftharpoons NO + N$	——	6.44E+14	−1	38,370
$NO + O \rightleftharpoons O_2 + N$	——	8.37E+09	0	19,450

Table A4 Forward reaction rate coefficients, $k_f(T_{eff}) = C_f T_{eff}^{\eta} \exp(-\theta_{ds}/T_{eff})$, Park[28]

Reaction	M	C_f, m^3/kmole · K$^{-\eta}$	η	Θ_{ds}, K
$N_2 + M \rightleftharpoons N + N + M$	N_2, O_2, NO	3.0E+18	−1.6	113,200
	N	3.0E+19	−1.6	113,200
	O	3.0E+19	−1.6	113,200
$O_2 + M \rightleftharpoons O + O + M$	N_2, O_2, NO	2.0E+18	−1.5	59,500
	N	1.0E+19	−1.5	59,500
	O	1.0E+19	−1.5	59,500
$NO + M \rightleftharpoons N + O + M$	N_2, O_2, NO	5.0E+12	0	75,500
	N	1.1E+14	0	75,500
	O	1.1E+14	0	75,500
$N_2 + O \rightleftharpoons NO + N$	——	6.4E+14	−1	38,400
$NO + O \rightleftharpoons O_2 + N$	——	8.4E+09	0	19,450

Acknowledgments

This research was supported under Air Force Office of Scientific Research contracts monitored by R. Canfield and S. Walker. We are thankful to G. V. Candler for discussions on transport properties, P. A. Gnoffo for performing the validation computation using the code LAURA, and M. Furudate for pointing out dissociation rates for the Park[1] model in the literature. The major part of computer resources were provided by the Department of Defense High Performance Computing Major Shared Resource Center at the U.S. Naval Oceanigraphic Office, Bay St. Louis, Mississippi and U.S. Army Research Laboratory Aberdeen Proving Grounds, Maryland.

References

[1]Park, C., *Nonequilibrium Hypersonic Aerothermodynamics*, Wiley, New York, 1990, Chaps. 3, 6.

[2]Osipov, A. I., and Stupochenko, E. V., "Kinetics of the Thermal Dissociation of Diatomic Molecules I. Small Impurity of Diatomic Molecules in a Monoatomic Inert Gas," *Combustion, Explosion and Shock Waves* (translated from *Fizika Goreniya i Vzryva*), Vol. 10, No. 3, 1974, pp. 303–313.

[3]Adamovich, I. V., Macheret, S. O., Rich, J. W., and Treanor, C. E., "Vibrational Relaxation and Dissociation Behind Shock Waves Part 2: Master Equation Modeling," *AIAA Journal*, Vol. 33, No. 6, 1995, pp. 1070–1075.

[4]Capitelli, M., Armenise, I., and Gorse, C., "State-to-State Approach in the Kinetics of Air Components Under Reentry Conditions," *Journal of Thermophysics and Heat Transfer*, Vol. 11, No. 4, 1997, pp. 570–578.

[5]Candler, G. V., Olejniczak, J., and Harrold, B., "Detailed Simulation of Nitrogen Dissociation in Stagnation Regions," *Physics of Fluids*, Vol. 9, No. 7, 1997, pp. 2108–2117.

[6]Josyula, E., "Computational Study of Vibrationally Relaxing Gas Past Blunt Body in Hypersonic Flows," *Journal of Thermophysics and Heat Transfer*, Vol. 14, No. 1, 2000, pp. 18–26.

[7]Wegener, P. P., and Buzyna, G., "Experiments on Shock Stand-Off Distance in Non-EquilibriumFlow," *Journal of Fluid Mechanics*, Vol. 37, No. 2, 1969, pp. 325–335.

[8]Oertel, H., Jr., "Oxygen Vibrational and Dissociation Relaxation Behind Regular Reflected Shocks," *Journal of Fluid Mechanics*, Vol. 74, No. 3, 1976, pp. 477–495.

[9]Park, C., "On Convergence of Computation of Chemically Reacting Flows," AIAA Paper 85-0247, Jan. 1985.

[10]Park, C., "Assessment of Two-Temperature Kinetic Model for Ionizing Air," AIAA Paper 87-1574, 1987.

[11]Park, C., "Assessment of Two-Temperature Kinetic Model for Dissociating and Weakly Ionizing Nitrogen," AIAA Paper 86-1347, 1986.

[12]Furudate, M., Nonaka, S., and Sawada, K., "Behavior of Two-Temperature Model in Intermediate Hypersonic Regime," *Journal of Thermophysics and Heat Transfer*, Vol. 13, No. 4, 1999, pp. 424–430.

[13]Furudate, M., Suzuki, T., and Sawada, K., "Calculation of Intermediate Hypersonic Flow Using Multi-Temperature Model," AIAA Paper 2000-0343, Jan. 2000.

[14]Sharma, S. P., Huo, W. M., and Park, C., "The Rate Parameters for Coupled Vibration–Dissociation in a Generalized SSH Approximation," AIAA Paper 88-2714, 1988.

Table A5 Constants for computing equilibrium constants[a] used with dissociation rates[28] of Tables A3 and A4[b]

Reaction	A_{1m}	A_{2m}	A_{3m}	A_{4m}	A_{5m}
$N_2 + M \rightleftharpoons N + N + M$	1.53510	15.4216	1.2993	−11.494	−0.00698
$O_2 + M \rightleftharpoons 2O + M$	0.553880	16.275511	1.776300	−6.57200	0.031445
$NO + M \rightleftharpoons N + O + M$	0.558890	14.53108	0.553960	−7.53040	−0.014089
$N_2 + O \rightleftharpoons NO + N$	0.976460	0.890430	0.745720	−3.96420	0.007123
$NO + O \rightleftharpoons N + O_2$	0.004815	−1.74430	1.22270	−0.95824	0.045545

[a]Equilibrium constants for chemical reactions computed using $K_{eq} = \exp(A_{1m}Z + A_{2m} + A_{3m}\ln(1/Z) + A_{4m}/Z + A_{5m}/Z^2)$ where $Z = T_{eff}/10,000$ (T_{eff} is the rate controlling temperature in Kelvin).
[b]Here $k_b(T_{eff}) = k_f(T_{eff})/K_{eq}(T_{eff})$; K_{eq} units for the dissociation reactions are kmole/m^3, and the exchange reactions are dimensionless.

Table A6 Forward reaction rate coefficients, $k_f(T) = C_f T^{\eta} \exp(-\theta_{ds}/T)$, Oertel[8]

Reaction	M	C_f, m^3/kmole · K$^{-\eta}$	η	Θ_{ds}, K
$O_2 + M \rightleftharpoons O + O + M$	O_2	6.20E+21	−2.5	59,136
	O	4.00E+16	−1.0	59,136

[15]Landrum, D. B., "Simulation of Vibration–Dissociation Coupling in Nitrogen," Ph.D. Thesis, Dept. of Mechanical and Aerospace Engineering, North Carolina State Univ., Raleigh, NC, 1992.

[16]Landau, L., and Teller, E., "Zur Theorie der Schalldispersion," *Physikalische Zeitschrift der Sowjetunion*, Vol. 10, No. 1, 1936, pp. 34–43.

[17]Nonaka, S., Mizuno, H., Takayama, K., and Park, C., "Measurement of Shock-Standoff Distance for Sphere in Ballistic Range," *Journal of Thermophysics and Heat Transfer*, Vol. 14, No. 2, April 2000, pp. 225–229.

[18]Gnoffo, P. A., and Cheatwood, F. M., "Users Manual fo the Langley Aerothermodynamic Upwind Relaxation Algorithm (LAURA)," NASA TM 4674, NASA Langley Research Center, Hampton, VA, April 1996.

[19]Vincenti, W. G., and Kruger, C. H., Jr., *Introduction to Physical Gas Dynamics*, Wiley, New York, 1967, Chaps. 1, 7.

[20]Millikan, R. C., and White, D. R., "Systematics of Vibrational Relaxation," *Journal of Chemical Physics*, Vol. 39, No. 12, 1963, pp. 3209–3213.

[21]Capitelli, M., Gorse, C., and Billing, G. D., "V–V Pumping Up in Nonequilibrium Nitrogen: Effects on the Dissociation Rate," *Chemical Physics*, Vol. 52, No. 3, 1980, pp. 299–304.

[22]Billing, G. D., and Fisher, E. R., "VV and VT Rate Coefficients in Diatomic Nitrogen by a Quantum Classical Model," *Chemical Physics*, Vol. 43, No. 3, 1979, pp. 395–401.

[23]Doroshenko, V. M., Kudryavtsev, N. N., Novikov, S. S., and Smetanin, V. V., "Effect of the Formation of Vibrationally Excited Nitrogen Molecules in Atomic Recombination in a Boundary Layer on the Heat Transfer," *High Temperature (USSR)*, Vol. 28, No. 1, 1990, pp. 82–89.

[24]Billing, G. D., "VV and VT Rates in N_2–O_2 Collisions," *Chemical Physics*, Vol. 179, No. 3, 1994, pp. 463–467.

[25]Mnatsakanyan, A. K., and Naidis, G. V., "The Vibrational-Energy Balance in a Discharge in Air," *High Temperature (USSR)*, Vol. 4, No. 3, 1985, pp. 506–513.

[26]Huber, K. P., and Herzberg, G., *Constants of Diatomic Molecules*, Van Nostrand Reinhold, New York, 1979, pp. 420, 421.

[27]Armenise, I., Capitelli, M., Celiberto, R., Colonna, G., and Gorse, C., "The Effect of $N + N_2$ Collisions on the Non-Equilibrium Vibrational Distributions of Nitrogen Under Reentry Conditions," *Chemical Physics Letters*, Vol. 227, No. 1, 1994, pp. 157–163.

[28]Park, C., "Calculation of Real-Gas Effects on Blunt-Body Trim Angles," *AIAA Journal*, Vol. 30, No. 4, 1992, pp. 999–1006.

[29]Blottner, F. G., Johnson, M., and Ellis, M., "Chemically Reacting Viscous Flow Program for Multicomponent Gas Mixtures," Sandia National Labs., Albuquerque, NM, TR SC-RR-70-754, 1971.

[30]Bird, R. B., Stewart, W. E., and Lightfoot, E. N., *Transport Phenomena*, Wiley, New York, 1960, p. 502.

[31]Chapman, S., and Cowling, T. G., *The Mathematical Theory of Non-Uniform Gases*, Cambridge Univ. Press, New York, 1990, Chaps. 6, 14.

[32]Josyula, E., "Oxygen Atoms' Effect on Vibrational Relaxation of Nitrogen in Blunt-Body Flows," *Journal of Thermophysics and Heat Transfer*, Vol. 15, No. 1, 2001, pp. 106–115.

[33]Gnoffo, P. A., Gupta, R. N., and Shinn, J. L., "Conservation Equations and Physical Models for Hypersonic Air Flows in Thermal and Chemical Nonequilibrium," NASA TP 2867, NASA Langley Research Center, Hampton, VA, Feb. 1989.